Supporting Information for:

Composition-Tunable Formamidinium Lead Mixed Halide Perovskites via Solvent-Free Mechanochemical Synthesis: Decoding the Pb Environments using Solid-State NMR Spectroscopy

Abdelrahman M. Askar,[1§] Abhoy Karmakar,[2§] Guy M. Bernard,[2] Michelle Ha,[2] Victor V. Terskikh,[3]

*Benjamin D. Wiltshire,[1] Sahil Patel,[1] Jonathan Fleet,[1] Karthik Shankar,[1] and Vladimir K. Michaelis[2]**

1- Department of Electrical and Computer Engineering, University of Alberta, Edmonton, Alberta, Canada, T6G 1H9
2- Department of Chemistry, University of Alberta, Edmonton, Alberta, Canada, T6G 2G2
3- Department of Chemistry, University of Ottawa, Ottawa, Ontario, Canada, K1N 6N5

Table of Contents

Materials and Methods

All starting precursor materials and solvents were obtained from commercial sources and used without further purification: lead (II) iodide (99%), lead (II) bromide (+98%) and lead (II) chloride (99%) from ACROS Organics (Morris Plains, NJ, USA), formamidinium chloride (97% purity) and γ-butyrolactone (GBL) (> 99 %) from Sigma Aldrich (St. Louis, MO, USA), dimethyl sulfoxide (DMSO) and N,N-dimethylformamide (DMF) from Fischer Scientific (Canada), formamidinium iodide (FAI) and formamidinium bromide (FABr) from Dyesol LTD (Australia).

Synthesis of $FAPbX_3$ Polycrystalline Samples:

$FAPbI_3$:[1] A 0.8 M solution of FAI and PbI_2 in GBL was placed at 60 ˚C until fully dissolved and became a bright yellow solution. The solution was filtered using 0.2 μm filters, and then the solution was distributed to small vials with 2 ml of solution in each. The vials were placed in an oil bath at 100 ˚C. The crystals were left to grow for 3-4 hours, washed thoroughly with GBL and immediately dried with a N_2 flow. The crystals were then stored in dark under vacuum until further use.

$FAPbBr_3$:[1] A 1 M solution of FABr and $PbBr_2$ in a 1:1 (v/v) DMF:GBL was prepared at room temperature and it formed a clear transparent solution. The solution was filtered using 0.2 μm filters and distributed to small vials with 2 ml of solution in each. The vials were placed in an oil bath at 70 ˚C. The crystals were left to grow for 3-4 hours, washed thoroughly with DMF and immediately dried with a N_2 flow. The crystals were stored in a desiccator until further use.

$FAPbCl_3$: A 0.5 M solution of FACl and $PbCl_2$ was prepared in 2 ml of DMF followed by ultrasonication at room temperature until it was fully dissolved. The resulting solution was clear. Then, the $FAPbCl_3$ solution was used to make films through a drop-cast method on pre-cleaned substrates

(using 150 μL of the solution on a 2 × 2 cm substrate), which were preheated to 65 ˚C. $FAPbCl_3$ formed quickly, within ~ 20 seconds. The substrates were left to dry for 30 minutes at 65 ˚C. Then, the powder was collected from substrates and phase purity was confirmed by XRD. Note that the formation of pure phase $FAPbCl_3$ is extremely sensitive to the quality of FACl, which is aggressively hygroscopic. $FAPbCl_3$ was accompanied by other phases when the FACl was not dry enough (see Figures S24 and S25).

Synthesis of MHPs - $FAPb(X_xX'_{1-x})_3$ Using MCS Route:

To synthesize MHPs using MCS-HG, appropriate amounts of $FAPbX_3$ and $FAPbX'_3$ were loaded with molar ratios calculated to achieve the desired mixed halide composition. For example, to prepare $FAPb(Br_{0.75}Cl_{0.25})_3$, 245.99 mg of $FAPbBr_3$ was mixed with 59.77 mg of $FAPbCl_3$. The mixing process by hand grinding continued until a fine powder with uniform color was achieved. The product was examined by XRD to make sure a single pure phase of MHP was obtained. Similarly, for the MCS-BM route, a Retsch PM100 planetary ball-milling instrument was used with 250 ml ZrO_2 container and different sized ZrO_2 beads. The rotation speed was 400 rpm, with 1 minute/2 sec on/off ratio and the rotation reversed after each cycle. All the synthesis experiments were undertaken under ambient lab conditions. We note that during the MCS-BM process, the temperature within the container was approximately 50 °C after the BM synthesis procedure due to friction.

Synthesis of MHPs - $FAPb(X_xX'_{1-x})_3$ Using Solvent Synthesis Route:

To synthesis $FAPb(Cl_xBr_{1-x})_3$ MHPs using solvent synthesis route, the drop-casting method was used. To prepare $FAPb(Br_{0.75}Cl_{0.25})_3$, stoichiometric amounts of FABr (62.49 mg), FACl (120.78 mg), and $PbBr_2$ (734.02 mg) were dissolved at room temperature in 2 ml of DMF to yield a 1 M solution, then drop casted on pre-heated clean glass substrates at 60 ˚C and left for drying in ambient air for 0.5 to 1 h. The formed film was collected and examined by XRD and a single crystallographic pure phase was obtained. For the solvent synthesis of $FAPb(Br_{0.50}I_{0.50})_3$, a precipitation technique was followed, which is a similar procedure to that used elsewhere[2] to prepare $MAPb(Br_{0.50}I_{0.50})_3$. Briefly, a mixture of PbI_2 (0.072 mmol), FAI (0.216 mmol), $PbBr_2$ (0.072 mmol), and FABr (0.216 mmol) were dissolved in a mixture of acetonitrile (20 mL) and DMF (200 μL), followed by precipitation via the addition of excess toluene. The product was then collected and dried under vacuum.

Reflectance Measurements of MHP Solid Samples

A Cary 400 UV-Vis spectrometer was used to obtain reflectance measurements on all powder samples. A black boat was loaded with approximately 100 mg of the sample in each measurement. The wavelength range was from 300 to 900 nm.

Powder XRD Measurements

Powder XRD patterns were collected on fine powders of each sample under identical conditions using a Bruker D8 Advance Diffractometer equipped with a Cu-Kα source and Vantec-500 2D detector. A 2θ scan between 10° and 60° was used. A pre-cleaned glass slide was used as the substrate. The refinements of powder XRD data were carried out using the software FullProf Suite, to determine the cell constants.

Solid-State Nuclear Magnetic Resonance Spectroscopy

^{1}H NMR spectra of MAS samples were acquired at 7.05 T (^{1}H, 300.4 MHz) on a Bruker Avance 300 NMR spectrometer with a Bloch pulse using a 4.0 μs π/2 pulse ($\gamma B_1/2\pi$ = 62.5 kHz) with a recycle delay of 60 s. Samples were packed in 4 mm o.d. zirconia rotors and spectra were acquired using a magic-angle spinning (MAS) frequency of 12 kHz. All ^{1}H spectra were referenced to TMS ($\delta(^{1}H)$ = 0.00 ppm) by setting the ^{1}H peak of adamantane to 1.85 ppm.[3]

^{13}C NMR spectra of MAS samples were acquired at 7.05 T on a Bruker Avance 300 NMR spectrometer equipped with a 4 mm double resonance MAS NMR probe. Samples were packed in 4 mm zirconia rotors and ^{13}C (ν_L = 75.5 MHz) cross-polarization (CP)[4] MAS NMR spectra were acquired with a spinning frequency of 5 kHz, a 4.0 μs π/2 pulse ($\gamma B_1/2\pi$ = 62.5 kHz), a contact time of 3.5 ms, and a recycle delay time of 60 s. All ^{13}C spectra were referenced to TMS ($\delta(^{13}C)$ = 0.00 ppm) by setting the high frequency ^{13}C peak of solid adamantane to 38.56 ppm.[5] All spectra were acquired with TPPM high power ^{1}H decoupling ($\gamma B_1/2\pi$ = 62.5 kHz).[6]

^{207}Pb NMR spectra for non-spinning samples were acquired at 7.05, 11.75 and 21.10 T on Bruker Avance 300, 500 and Avance II 900 NMR spectrometers, respectively. The samples were packed in 4 mm zirconia rotors and ^{207}Pb NMR spectra were collected using a 4 mm double resonance H/X Bruker probe, using either a Hahn-echo[7] ($(\pi/2)_x - \tau_1 - (\pi)_y - \tau_2 -$ ACQ, where τ represents the inter-pulse and refocusing delay) or a modified Hahn-echo pulse sequence, whereby the second pulse is replaced with a π/2 pulse to achieve broader excitation width at higher magnetic field strengths. The spin-lattice relaxation times (T_1) of ^{207}Pb nuclei were measured for all samples using a modified inversion recovery sequence incorporating a refocusing pulse ($\pi - \tau_1 - \pi/2 - \tau_2 - \pi/2 - \tau_2 -$ ACQ), where τ_1 is the variable

delay used to access the inverse recovery and τ_2 (30 μs here) is the delay typically used in a solid-echo sequence. The T_1 values were obtained by fitting the peak intensity optima values to a three-parameter exponential decay function. A value of 5-10 s of recycle delays were used for each sample based on the T_1 value of that sample (Table 1). We used the variable offset cumulative spectra (VOCS)[8] approach with between 3 and 5 steps and a 30 kHz (for 7.05 and 11.75 T) or 50 kHz (for 21.1 T) transmitter stepping frequency across the spectral range to ensure acquisition of the complete, undistorted spectrum; the sub-spectra were added using the skyline projection method. Two-dimensional ^{207}Pb EXSY[9] NMR spectra were acquired using mixing times of 10 μs, 50 μs and 2 ms. A total of 64 slices were collected in the indirect dimension using a 2 μs increment, and between 2k and 3k transients were acquired per slice. All ^{207}Pb NMR spectra were referenced to $PbMe_4$ ($\delta(^{207}Pb)$ = 0.00 ppm) by setting the ^{207}Pb peak of solid $MAPbCl_3$ measured at 293 K to −647.5 ppm.[10] All spectra were processed using Topspin 3.5 Bruker software with between 250 and 500 Hz exponential apodization and plotted using OriginPro 8 software. ^{207}Pb NMR spectra for $FAPbX_3$ (X = Cl, Br, I) were fit using the WSOLIDS software[11] with guidance on the chemical shielding anisotropy contributions obtained from the results of DFT magnetic shielding calculations (vide infra). The isotropic chemical shift (δ_{iso}) values for the ^{207}Pb spectra were not clearly defined due to the complex broad peaks (except for δ-phase of $FAPbI_3$), thus, here we report a chemical shift (δ_{cs}) value, which is the center of mass of the powder pattern.

We note that under MAS conditions, the line widths only narrow marginally due to the removal of the heteronuclear dipole couplings between Pb and X. High power proton decoupling was attempted, however did not show significant differences in the overall line shape or width; this is attributed to the fast motion of the FA cation (reorientation times ~ 8 ps at room temperature)[12] within the until cell and therefore its ^{1}H nuclei self-decouple from the Pb. Site resolution increased at higher magnetic field strengths.

^{207}Pb NMR of non-spinning δ-$FAPbI_3$ exhibited a magnetic shielding anisotropy, the experimental data was fit using WSOLIDS implementing the Maryland Convention[13] method where the isotropic chemical shift, span and skew are defined as, $\delta_{iso} = (\delta_{11} + \delta_{22} + \delta_{33})/3$; $\Omega = \delta_{11} - \delta_{33}$ and $\kappa = 3(\delta_{22} - \delta_{iso})/\Omega$, respectively.

<u>Quantum Chemical Calculations:</u>

Density functional theory (DFT) calculations of the Pb magnetic shielding on a series of ten $[PbBr_xI_{6-x}]^{4-}$ octahedral model anions were carried out using the Amsterdam Density Functional (ADF) 2017 modeling suite.[14-17] The structures were modeled by assuming octahedral coordination about the Pb, with a bond length for Pb-Br of 2.966 Å and Pb-I of 3.146 Å, derived from XRD data.[17] Relativistic effects were incorporated using the zeroth order regular approximation (ZORA) method along with the ZORA/QZ4P basis set, which is optimized for relativistic calculations.[18, 19] All principal components of the calculated ^{207}Pb magnetic shielding tensors are available in the supporting information and are defined using the Maryland Convention.[13, 20] All DFT calculations used the Perdew, Burke, and Ernzerhof (PBE) functional in the generalized gradient approximation (GGA).[21-23]

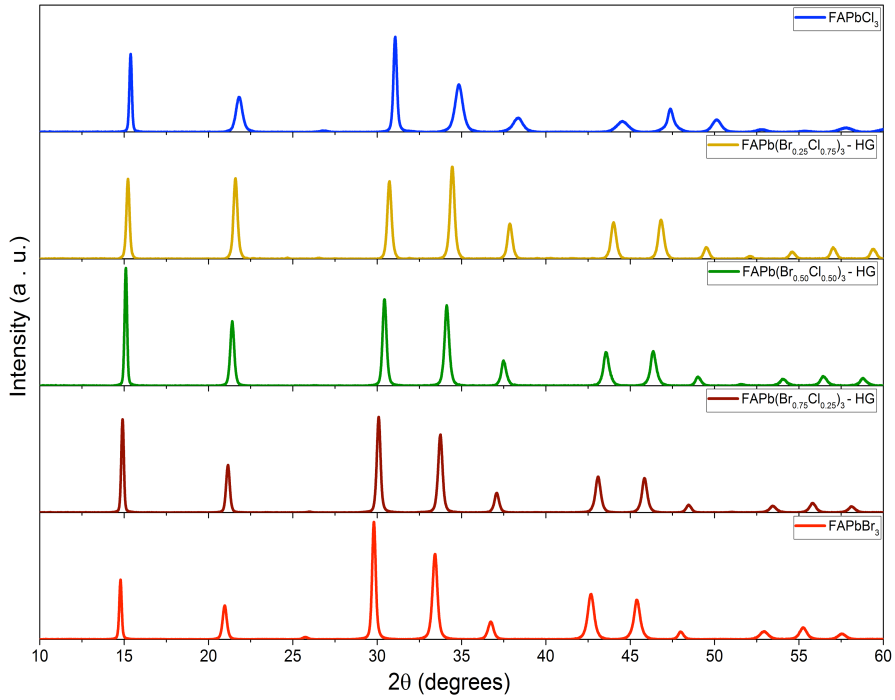

Figure S1. *Powder XRD patterns for the MCS HG-FAPb(Cl_xBr_{1-x})$_3$ series of samples.*

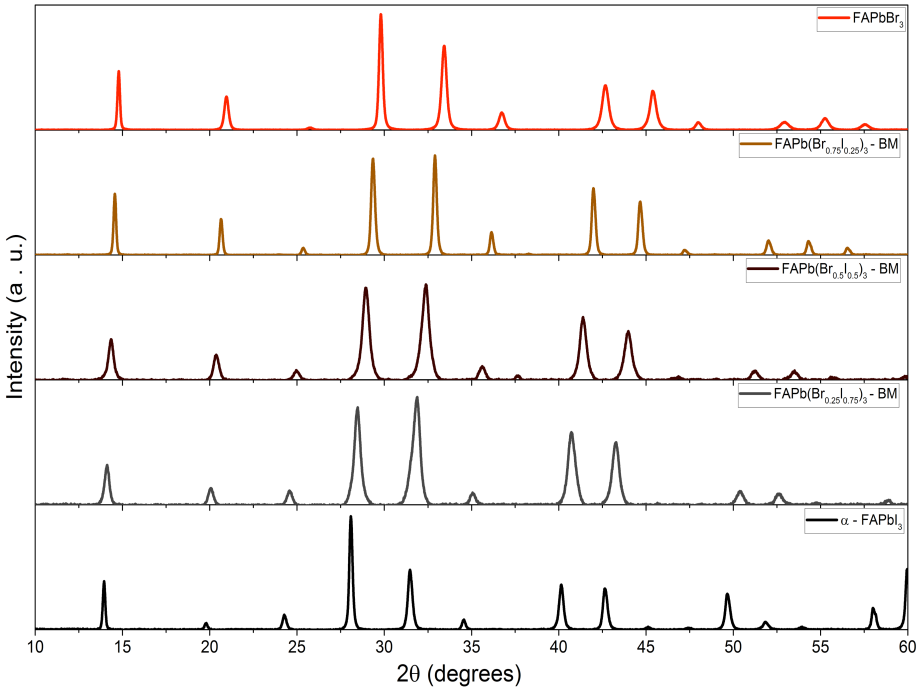

Figure S2. *Powder XRD patterns for the MCS BM-FAPb(Br_xI_{1-x})$_3$ series of samples.*

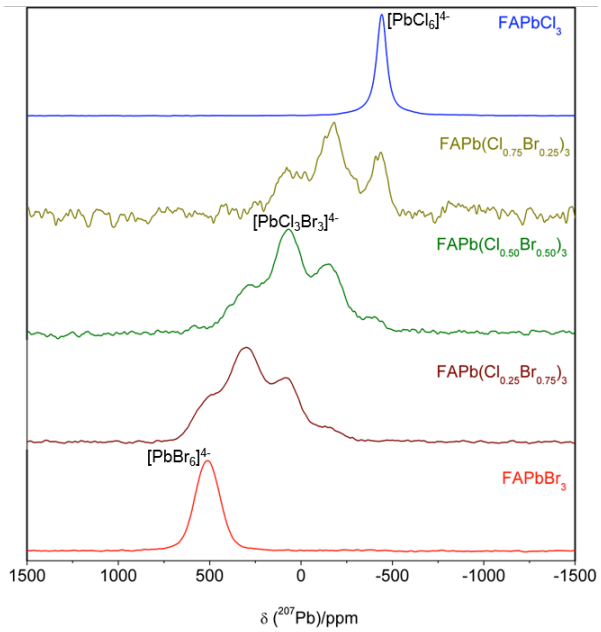

Figure S3. *^{207}Pb NMR spectra for non-spinning $FAPb(Cl_xBr_{1-x})_3$ prepared by HG, where x = 0.75, 0.50, and 0.25, along with those for the parent compounds, $FAPbCl_3$ and $FAPbBr_3$, acquired at 11.75 T.*

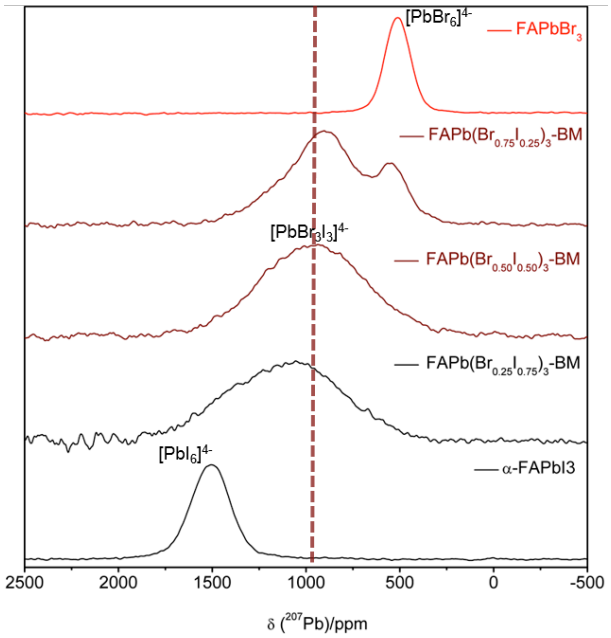

Figure S4. *^{207}Pb NMR spectra for non-spinning $FAPb(Br_xI_{1-x})_3$ prepared by BM, where x = 0.75, 0.50, and 0.25, along with those for the parent compounds, $FAPbBr_3$ and α-$FAPbI_3$ acquired at 11.75 T.*

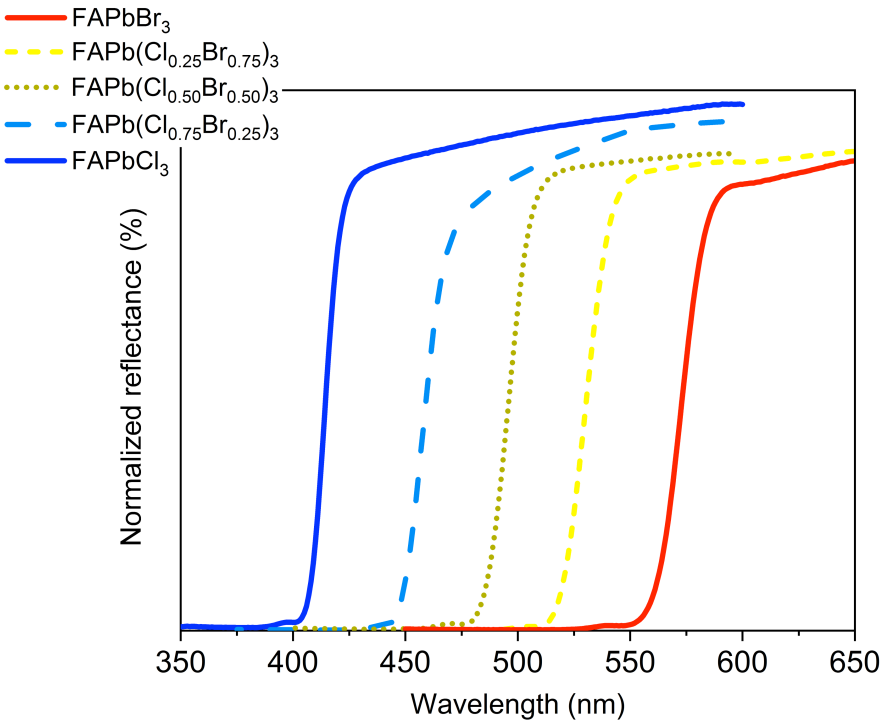

Figure S5. *Reflectance spectra for $FAPb(Cl_xBr_{1-x})_3$ prepared by HG, where x = 0.75, 0.50, and 0.25, along with those for the parent compounds, $FAPbCl_3$ and $FAPbBr_3$.*

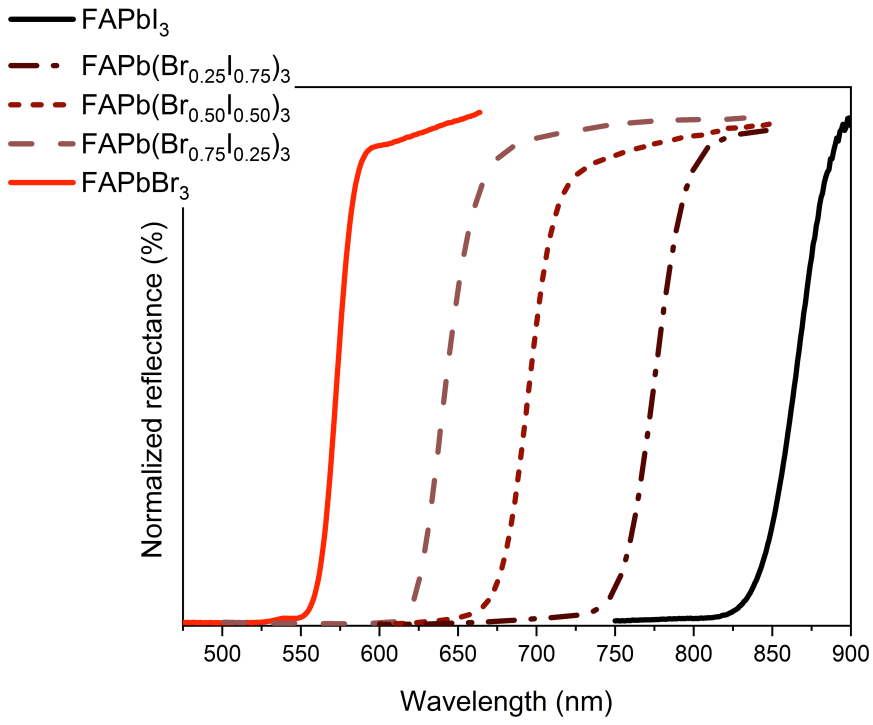

Figure S6. *Reflectance spectra for $FAPb(Br_xI_{1-x})_3$ prepared by BM, where x = 0.75, 0.50, and 0.25, along with those for the parent compounds, $FAPbBr_3$ and α-$FAPbI_3$.*

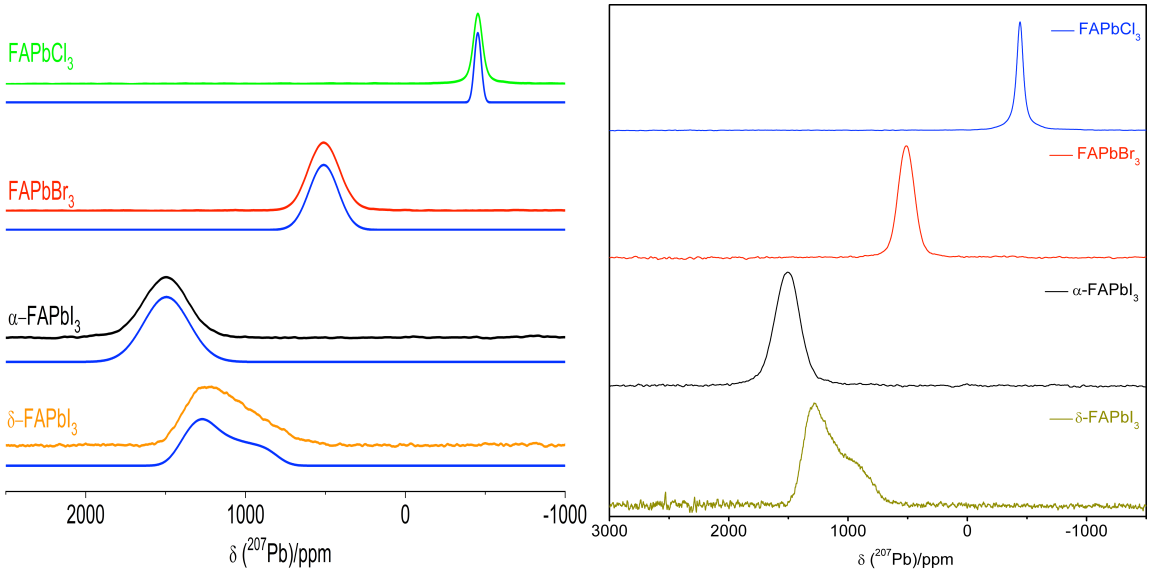

Figure S7. *^{207}Pb NMR spectra for the three non-spinning $FAPbX_3$ parent compounds and for δ-$FAPbI_3$ acquired at 7.05 T; simulated spectra (blue traces) are shown below the experimental spectra (left). ^{207}Pb NMR spectra for the three $FAPbX_3$ parent compounds and for δ-$FAPbI_3$ acquired at 11.75 T (right).*

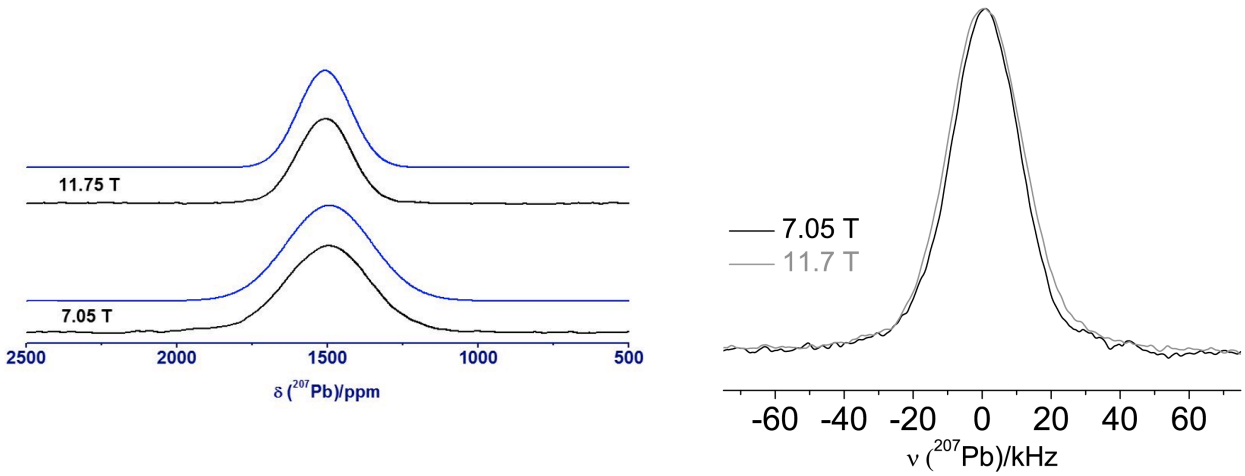

Figure S8. *Experimental (black lines) and simulated (blue lines) ^{207}Pb NMR spectra of non-spinning α-$FAPbI_3$ acquired at 7.05 and 11.75 T (ppm, left). 7.05 T – FWHM ~350 ppm (~22 kHz) and 11.75 T – FWHM ~210 ppm (~22 kHz). Overlay of ^{207}Pb NMR spectra at 7.05 and 11.75 T (kHz, right).*

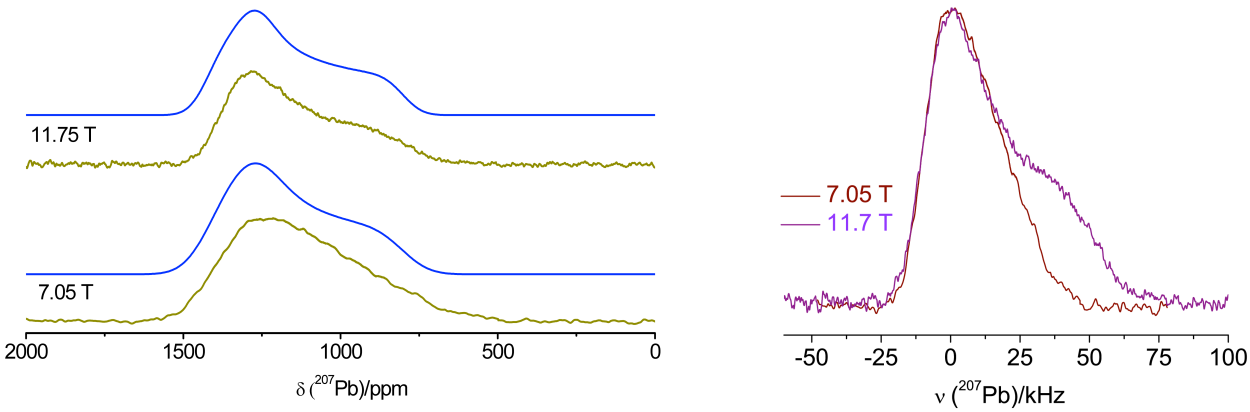

Figure S9. *Comparison between ^{207}Pb NMR spectra for non-spinning δ-FAPbI$_3$ acquired at 7.05 and 11.75 T (ppm (left) and kHz (right)), along with simulated (blue traces) spectra.*

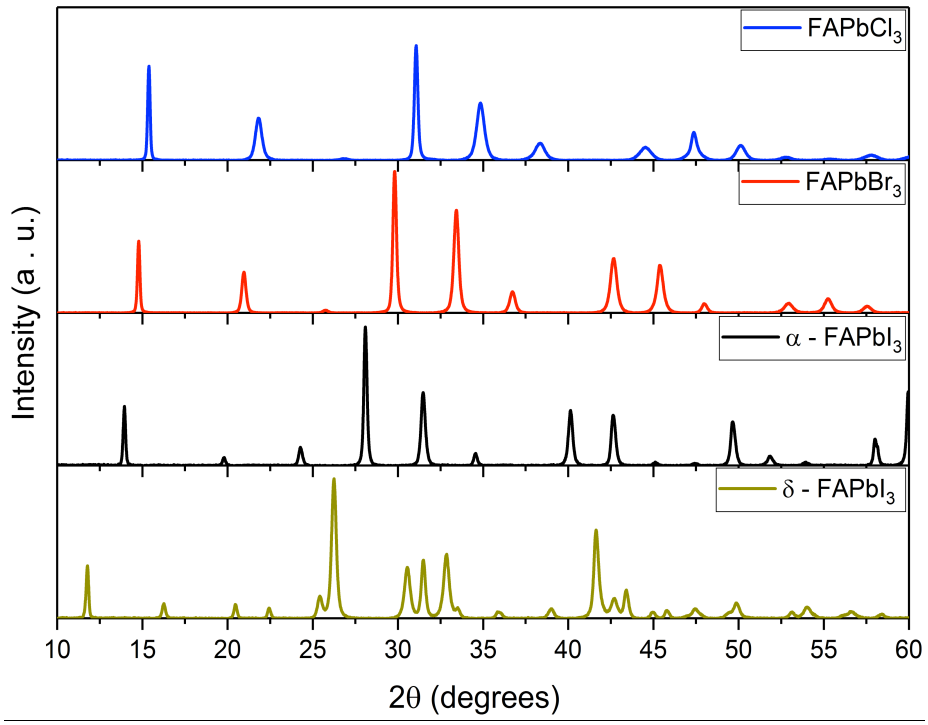

Figure S10. *Powder XRD comparison for the three FAPbX$_3$ parent compounds, along with the δ-FAPbI$_3$ obtained by leaving black α-FAPbI$_3$ crystalline powder sample in a humid environment for two days they become totally yellow.*

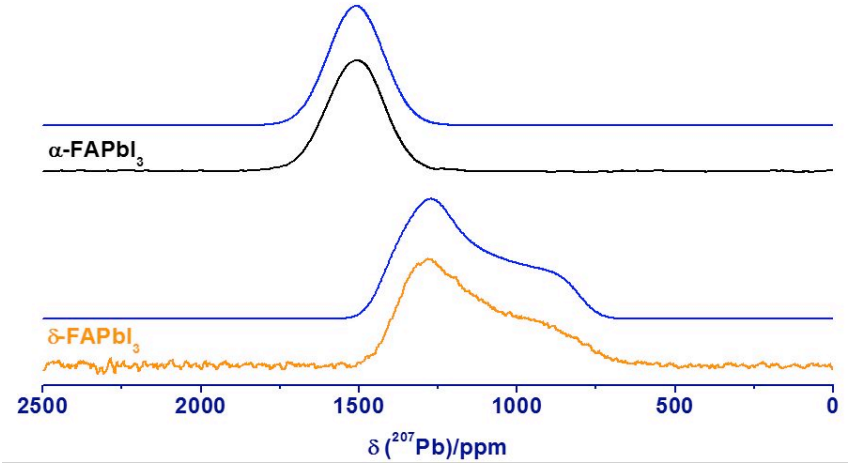

Figure S12. *Experimental (black / yellow) and simulated (blue traces)* ^{207}*Pb NMR spectra of non-spinning α-FAPbI*$_3$ *and δ-FAPbI*$_3$ *acquired at 11.75 T.*

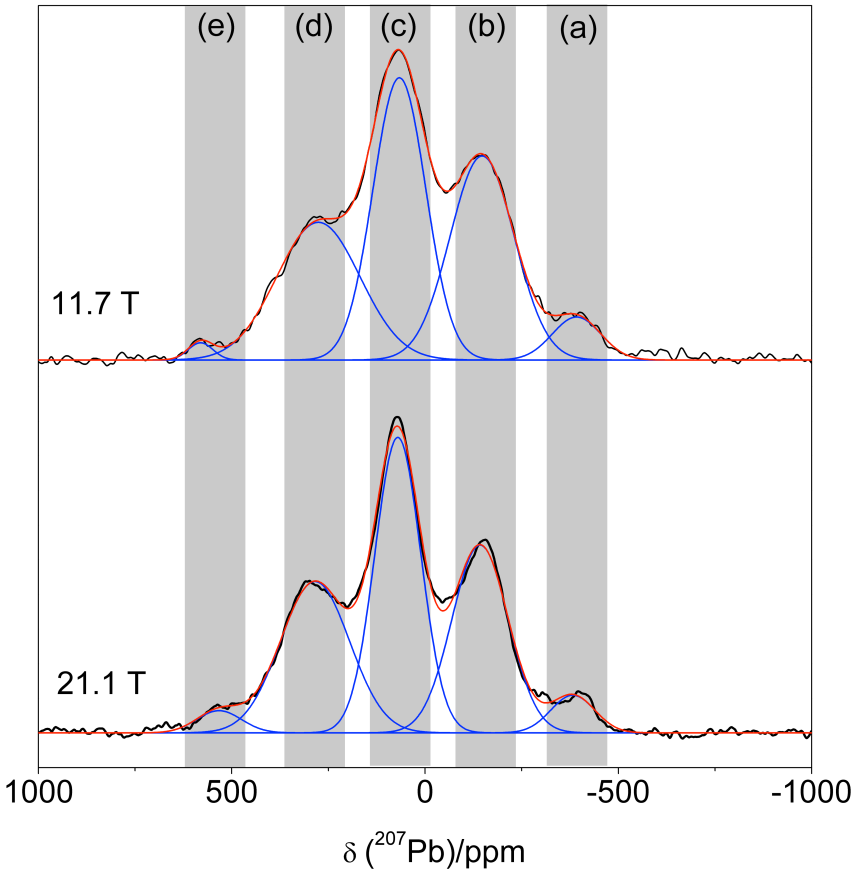

Figure S12. ^{207}*Pb NMR spectra for non-spinning HG-FAPb(Cl*$_{0.5}$*Br*$_{0.5}$*)*$_3$ *acquired at 11.75 and 21.1 T, with peak fitting assuming a simple Gaussian lineshape.* $[PbCl_6]^{4-}$ *(a);* $[PbCl_5Br]^{4-}$*/*$[PbCl_4Br_2]^{4-}$ *(b);* $[PbCl_3Br_3]^{4-}$ *(c);* $[PbCl_2Br_4]^{4-}$*/*$[PbClBr_5]^{4-}$ *(d);* $[PbBr_6]^{4-}$ *(e).*

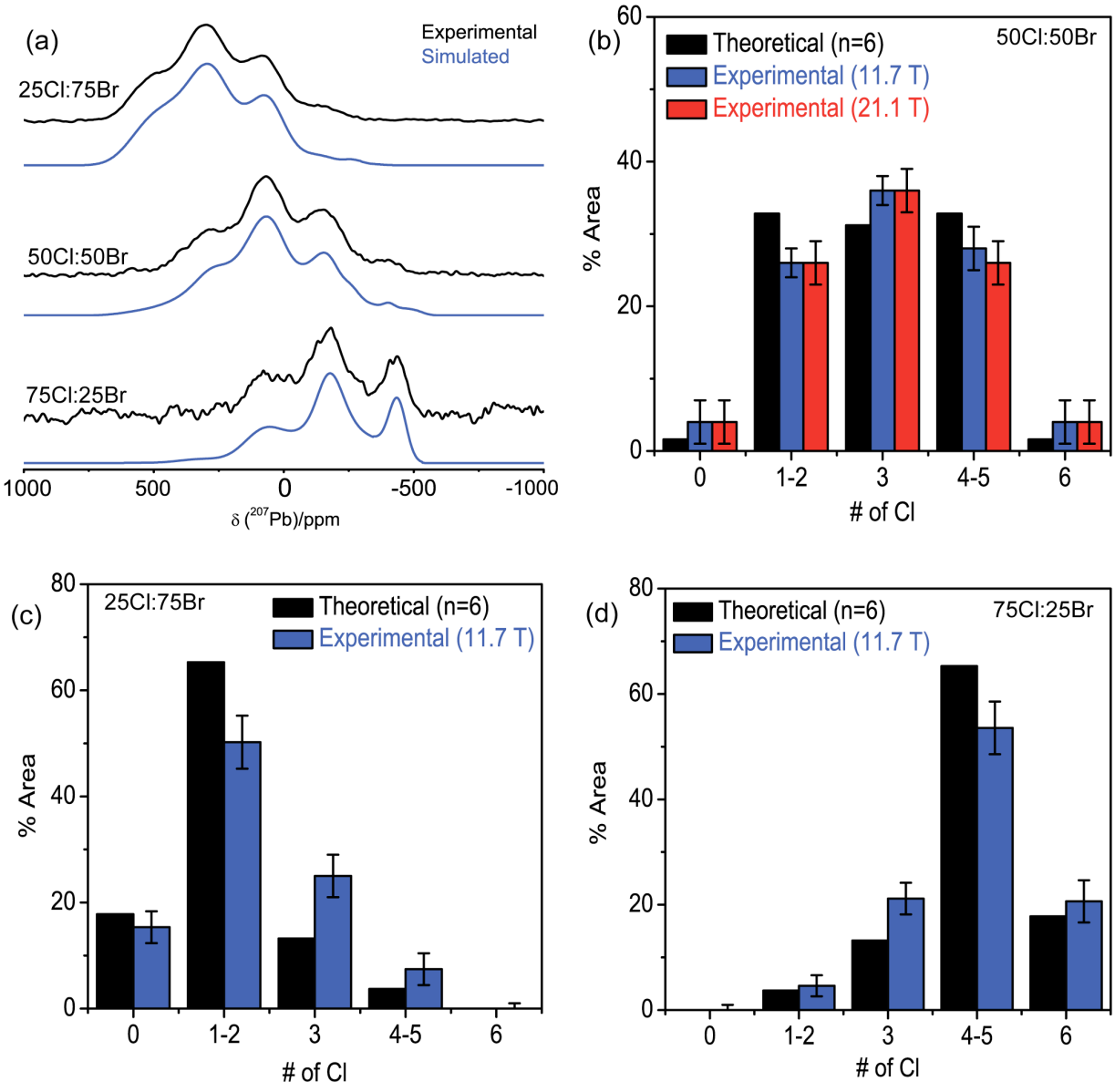

Figure S13. *^{207}Pb NMR spectra and the binomial distribution for non-spinning HG-FAPb(Cl_xBr_{1-x})$_3$ based on the curve fitting of the ^{207}Pb NMR acquired at 11.75 and 21.1 T. Error bars shown here are based on a comparison of the simulated and experimental spectra. (a) ^{207}Pb NMR spectra at 11.75 T for HG-FAPb(Cl_xBr_{1-x})$_3$ with fitted curves using insight from the DFT data. (b) Comparison between theoretical binomial distributions based on 7 different sites (n = 6) and the population distribution for HG-FAPb($Cl_{0.5}Br_{0.5}$)$_3$ extracted from area under curve for ^{207}Pb NMR spectra acquired at 11.75 and 21.1 T. (c and d) As for (b), but for HG-FAPb($Cl_{0.25}$ $Br_{0.75}$)$_3$ and HG-FAPb($Cl_{0.75}$ $Br_{0.25}$)$_3$, respectively with data obtained at 11.75 T.*

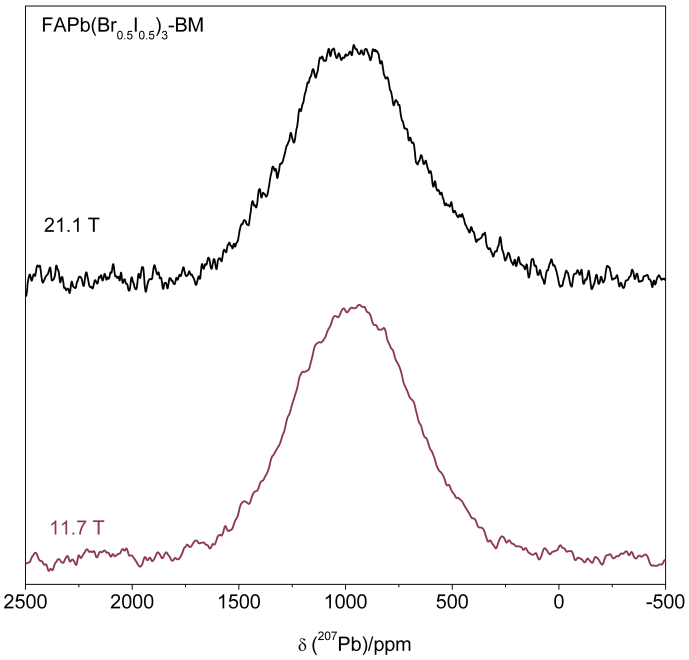

Figure S14. *Comparison between ^{207}Pb NMR spectra for non-spinning MCS BM-FAPb($Br_{0.5}I_{0.5}$)$_3$ acquired at 11.75 and 21.1 T.*

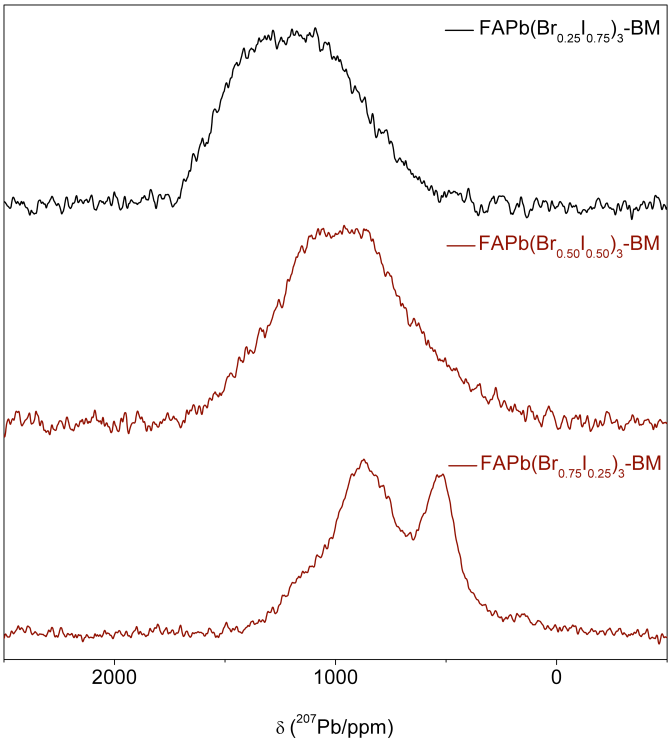

Figure S15. *^{207}Pb NMR spectra for the non-spinning MCS BM-FAPb(Br_xI_{1-x})$_3$ series of samples acquired at 21.1 T.*

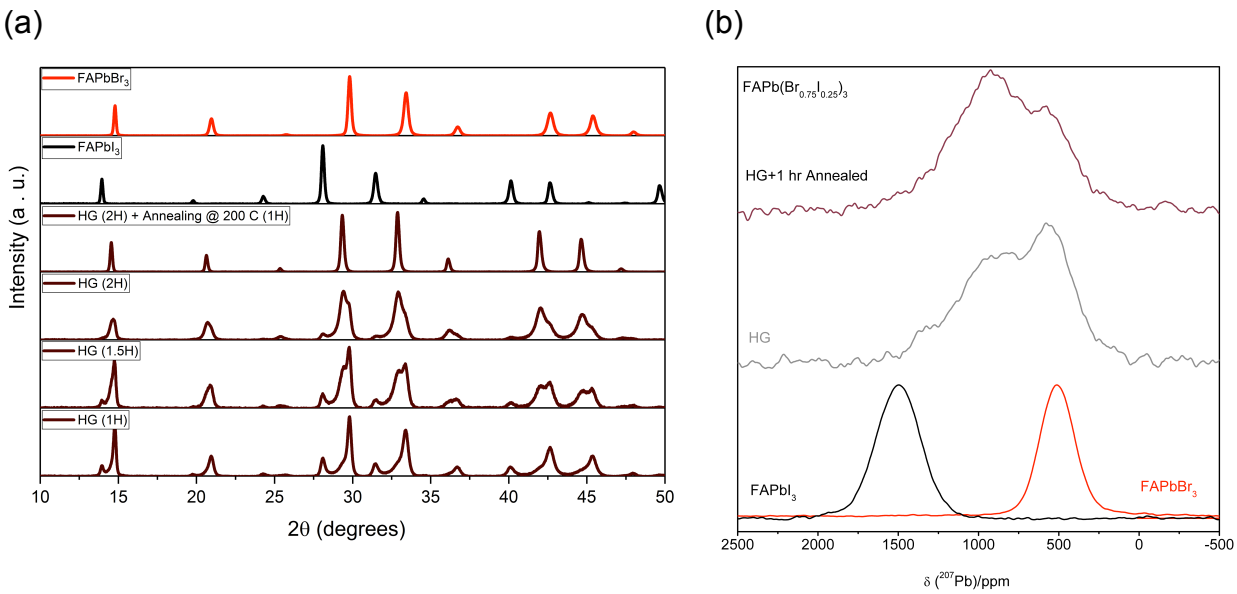

Figure S16. *(a) Powder XRD comparison of $FAPb(Br_{0.75}I_{0.25})_3$ prepared by HG at different time stamps and after an additional 1 h of annealing at 200 ˚C, along with those for the parent compounds, $FAPbBr_3$ and α-$FAPbI_3$. (b) Comparison between the ^{207}Pb NMR spectra of non-spinning $FAPb(Br_{0.75}I_{0.25})_3$ prepared by HG (2 h) before and after 1 h of annealing, along with those for the parent compounds, $FAPbBr_3$ and α-$FAPbI_3$.*

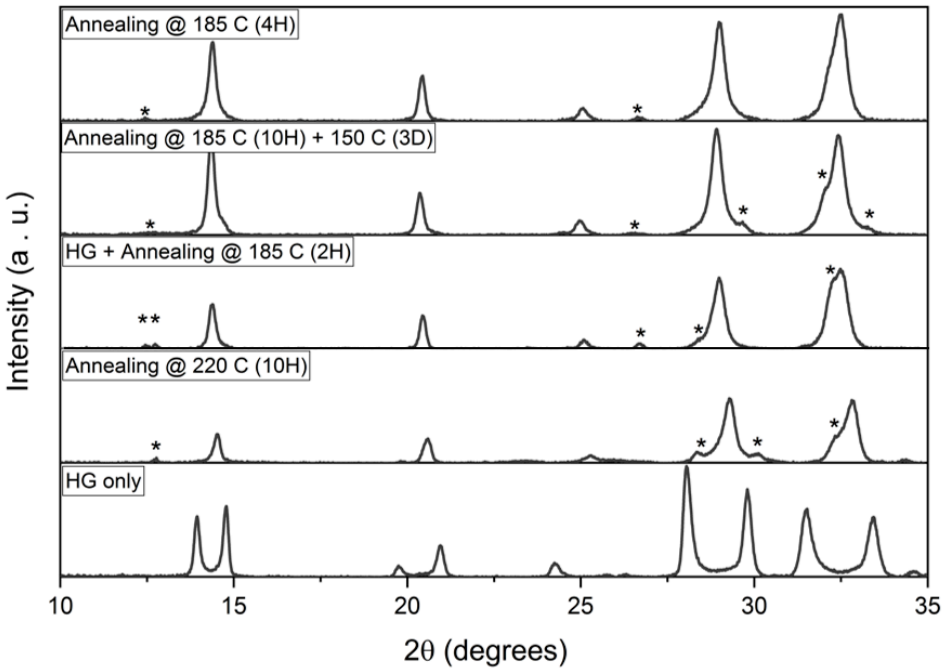

Figure S17. *Powder XRD spectra for various attempts to prepare $FAPb(Br_{0.5}I_{0.5})_3$ by HG and solid-state synthesis at elevated temperatures. Asterisks indicate peaks for either decomposition products, such as PbI_2 or for phases other than $FAPb(Br_{0.5}I_{0.5})_3$.*

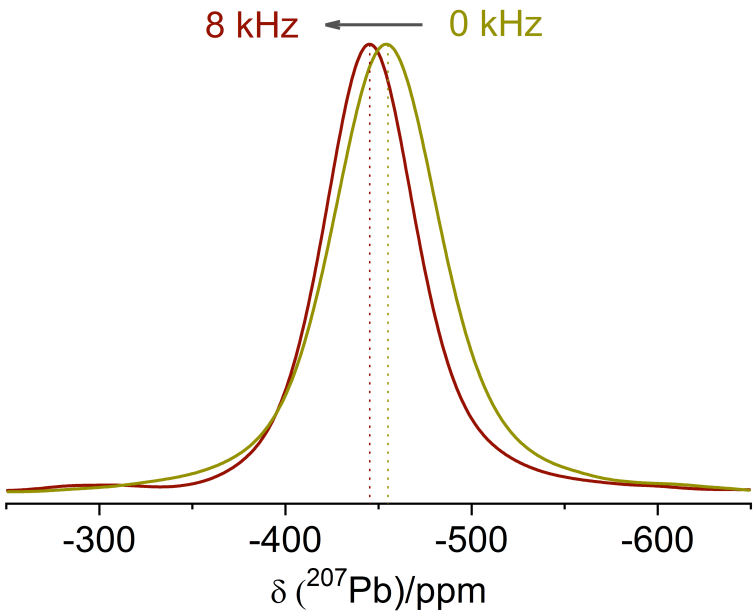

Figure S18. *Comparison of ^{207}Pb NMR spectra of non-spinning (gold) and MAS (8 kHz, brown) $FAPbCl_3$, showing a shift to higher frequency with MAS and a ~9% narrowing at the full width at half maximum. The narrowing is attributed to removal by MAS of the effects of minor heteronuclear dipolar coupling interactions while the shift to higher frequency arises from sample heating during MAS.*[10]

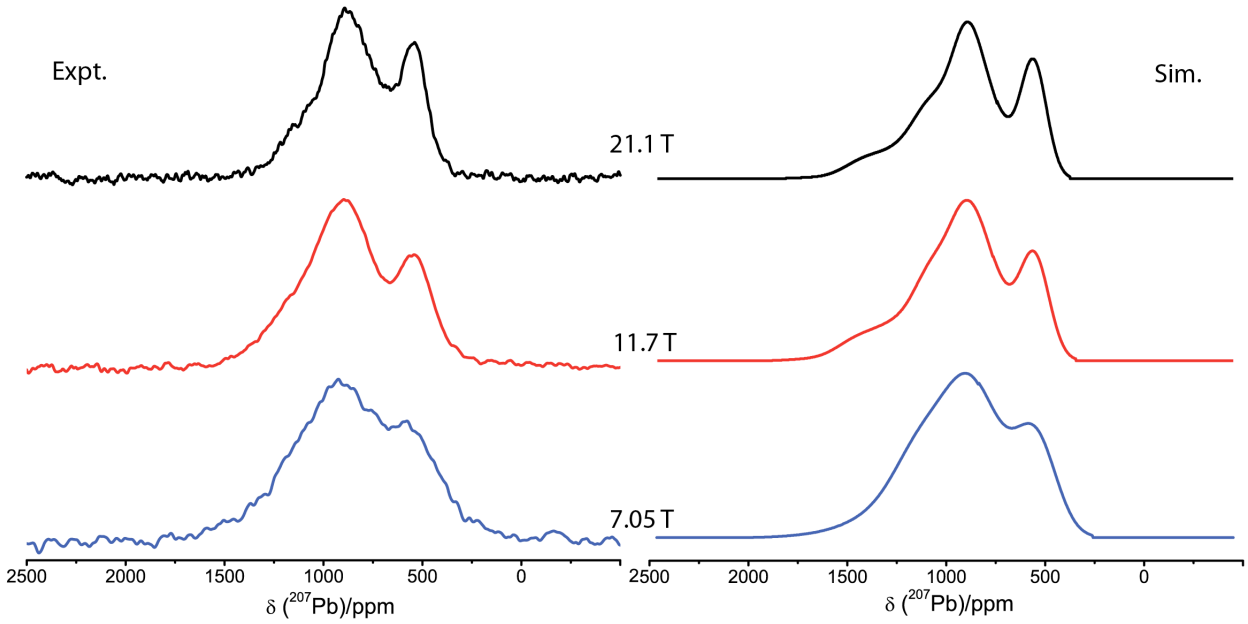

Figure S19. *Comparison between the ^{207}Pb NMR spectra of non-spinning $FAPb(Br_{0.75}I_{0.25})_3$ prepared by HG+1 hr annealing at 7.05, 11.75, and 21.1 T with associated spectral simulations using DFT predicted NMR parameters of $[PbBr_xI_{6-x}]^{4-}$ where x = 0 – 6 using a binomial-like distribution.*

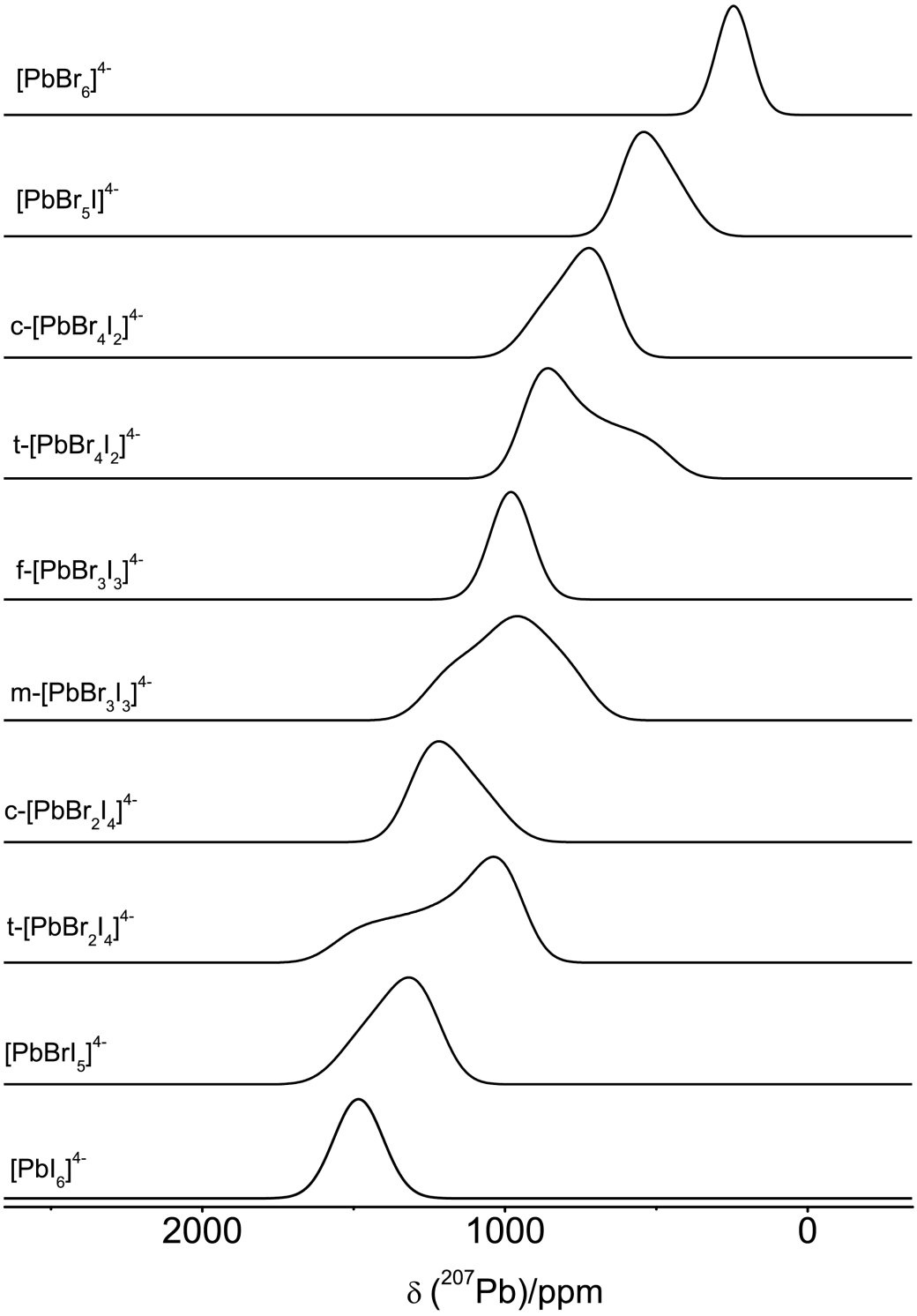

Figure S20. *Simulated ^{207}Pb NMR spectra for $[PbBr_xI_{6-x}]^{4-}$ octahedra based on DFT-calculated $\delta(^{207}Pb)$. Please note c = cis, t = trans, f = fac and m = mer.*

The FA cation resides at the cubooctahedral position of the unit cell but is not directly bonded to the halide atoms (dynamic in nature) and thus the isotropic ^{1}H and ^{13}C chemical shifts are not significantly influenced by the halide environment. ^{13}C NMR resonances are nearly identical in position and line width for all parent compounds (Figures S21 and S22). Though there are three unique ^{1}H nuclei present within a FA^{+}, at 7.05 T, a single Gaussian-like resonance is observed for the FA perovskite, due to ^{1}H homonuclear dipole coupling.[12] The ^{1}H isotopic chemical shifts (δ_{iso}) for all single halide perovskites are nearly identical while the line widths broaden slightly from chlorine to iodine (Figure S23).

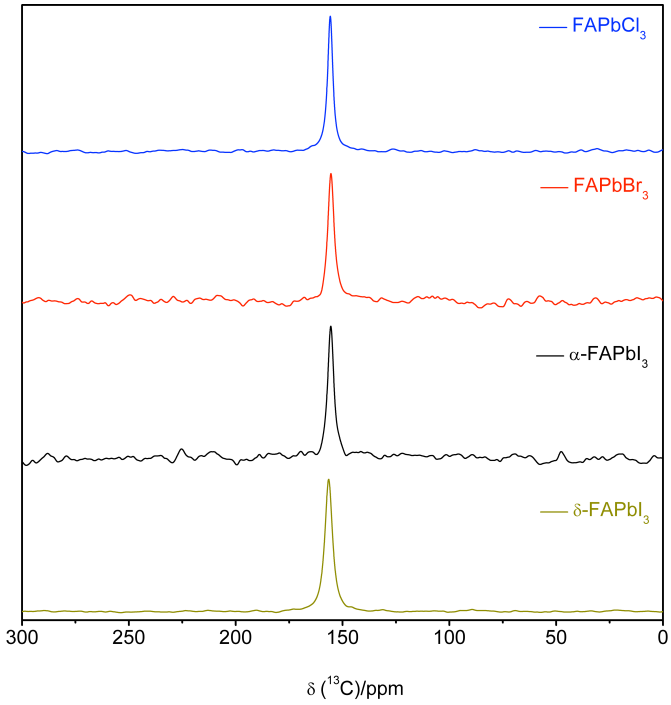

Figure S21. *Carbon-13 CP MAS NMR spectra for the three $FAPbX_3$ parent compounds, along with that for δ-$FAPbI_3$, acquired at 7.05 T with a spinning frequency of 5 kHz.*

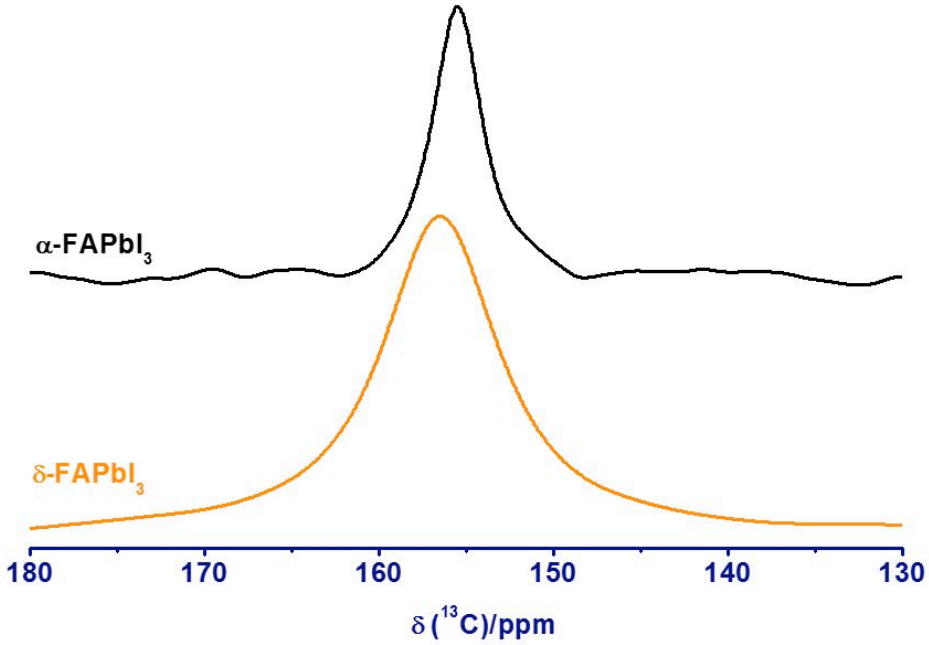

Figure S22. *Experimental ^{13}C CP MAS NMR spectra of α-$FAPbI_3$ (black) and δ-$FAPbI_3$ (yellow) at 7.05 T with 5 kHz spinning.*

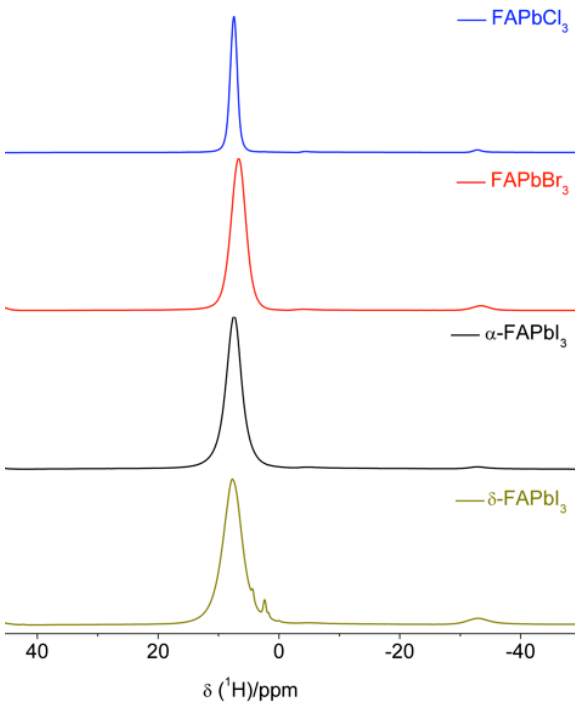

Figure S23. *^{1}H NMR spectra for the three MAS $FAPbX_3$ parent compounds, along with the δ-$FAPbI_3$ acquired at 7.05 T with a spinning frequency of 12 kHz. Spinning side bands are located at -32 ppm.*

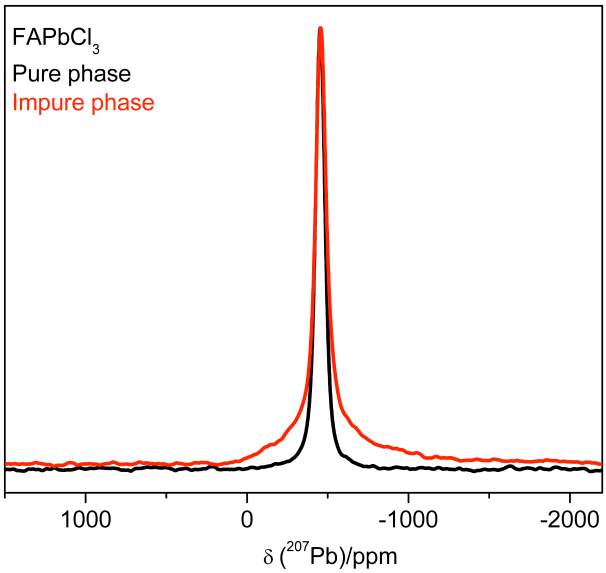

Figure S24. *^{207}Pb NMR spectra for non-spinning $FAPbCl_3$; (black) pure phase, (red) impure phase. Corresponding pXRD data for the impure sample is shown in Figure S25.*

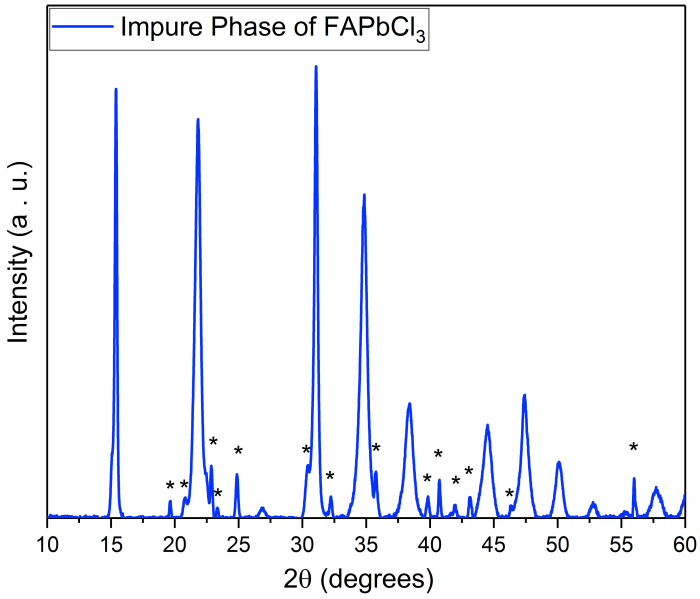

Figure S25. *Powder XRD for an impure phase of $FAPbCl_3$ obtained with low quality and not-well stored (hydrated) FACl. Powder-XRD peaks labeled with asterisks are for impure phase(s) other than $FAPbCl_3$.*

Table S1. *^{207}Pb magnetic shielding parameters from model anions $[PbBr_xI_{6-x}]^{4-}$ from DFT calculations*

DFT Model	No. of I	σ_{11} (ppm)	σ_{22} (ppm)	σ_{33} (ppm)	σ_{iso} (ppm)	Ω (ppm)	κ
$[PbBr_6]^{4-}$	0	8533.6	8533.6	8533.6	8533.6	0.0	0
$[PbBr_5I]^{4-}$	1	8191.6	8191.6	8404.7	8262.6	213.1	1.00
$[Pb\ Br_4I_2]^{4-}$ *-cis*	2	7845.0	8103.5	8108.9	8019.1	263.9	-0.96
$[PbBr_4I_2]^{4-}$ *-trans*	2	7871.5	7871.5	8328.1	8023.7	456.6	1.00
$[PbBr_3I_3]^{4-}$ *-fac*	3	7798.0	7799.4	7799.4	7798.9	1.4	-1.00
$[Pb\ Br_3I_3]^{4-}$ *-mer*	3	7518.1	7818.8	8055.0	7797.0	536.9	-0.12
$[Pb\ Br_2I_4]^{4-}$ *-cis*	4	7500.7	7520.0	7779.5	7597.3	278.8	0.93
$[PbBr_2I_4]^{4-}$ *-trans*	4	7214.9	7510.9	7797.3	7603.2	582.4	-1.00
$[PbBrI_5]^{4-}$	5	7235.0	7797.3	7520.0	7425.0	284.9	-1.00
$[PbI_6]^{4-}$	6	7294.9	7294.9	7294.9	7294.9	0.0	0

REFERENCES

1. Saidaminov, M. I.; Abdelhady, A. L.; Maculan, G.; Bakr, O. M. *ChemComm* **2015,** 51, (100), 17658-17661.
2. Rosales, B. A.; Men, L.; Cady, S. D.; Hanrahan, M. P.; Rossini, A. J.; Vela, J. *Chem. Mater.* **2016,** 28, (19), 6848-6859.
3. Hayashi, S.; Hayamizu, K. *Bul. Chem. Soc. Jap.* **1991,** 64, (2), 685-687.
4. Pines, A.; Gibby, M. G.; Waugh, J. S. *J. Chem. Phys.* **1972,** 56, (4), 1776-1777.
5. Earl, W. L.; Vanderhart, D. L. *J. Mag. Res. (1969)* **1982,** 48, (1), 35-54.
6. Bennett, A. E.; Rienstra, C. M.; Auger, M.; Lakshmi, K. V.; Griffin, R. G. *J. Chem. Phys.* **1995,** 103, (16), 6951-6958.
7. Hahn, E. L. *Phys. Rev.* **1950,** 80, (4), 580-594.
8. Massiot, D.; Farnan, I.; Gautier, N.; Trumeau, D.; Trokiner, A.; Coutures, J. P. *Solid State Nucl. Mag. Res.* **1995,** 4, (4), 241-248.
9. Jeener, J.; Meier, B. H.; Bachmann, P.; Ernst, R. R. *J. Chem. Phys.* **1979,** 71, (11), 4546-4553.
10. Bernard, G. M.; Goyal, A.; Miskolzie, M.; McKay, R.; Wu, Q.; Wasylishen, R. E.; Michaelis, V. K. *J. Mag. Res.* **2017,** 283, 14-21.
11. Eichele, K. *WSOLIDS NMR Simulation Package*, 1.21.3; Universität Tübingen: Tübingen, Germany, 2013.
12. Fabini, D. H.; Siaw, T. A.; Stoumpos, C. C.; Laurita, G.; Olds, D.; Page, K.; Hu, J. G.; Kanatzidis, M. G.; Han, S.; Seshadri, R. *J. Amer. Chem. Soc.* **2017,** 139, (46), 16875-16884.
13. Mason, J. *Solid State Nucl. Mag. Res.* **1993,** 2, (5), 285-288.
14. Te Velde, G.; Bickelhaupt, F. M.; Baerends, E. J.; Guerra, C. F.; van Gisbergen, S. J. A.; Snijders, J. G.; Ziegler, T. *J. Comp. Chem.* **2001,** 22, 931-967.
15. Fonseca Guerra, C.; Snijders, J. G.; Te Velde, G.; Baerends, E. J. *Theoret. Chem. Acc.* **1998,** 99, (6), 391-403.
16. Te Velde, G.; Bickelhaupt, F. M.; Baerends, E. J.; Fonseca Guerra, C.; van Gisbergen, S. J. A.; Snijders, J. G.; Ziegler, T. *J. Comp. Chem.* **2001,** 22, (9), 931-967.
17. Jaffe, A.; Lin, Y.; Beavers, C. M.; Voss, J.; Mao, W. L.; Karunadasa, H. I. *ACS Central Sci.* **2016,** 2, (4), 201-209.
18. Lenthe, E. v.; Ehlers, A.; Baerends, E.-J. *J. Chem. Phys.* **1999,** 110, (18), 8943-8953.
19. Schreckenbach, G.; Ziegler, T. *J. Phys. Chem.* **1995,** 99, (2), 606-611.
20. Herzfeld, J.; Berger, A. E. *J. Chem. Phys.* **1980,** 73, (12), 6021-6030.
21. Perdew, J. P.; Burke, K.; Ernzerhof, M. *Phys. Rev. Lett.* **1996,** 77, 3865.
22. Perdew, J. P.; Burke, K.; Ernzerhof, M. *Phys. Rev. Lett.* **1998,** 80, 891.
23. Perdew, J. P.; Burke, K.; Ernzerhof, M. *Phys. Rev. Lett.* **1997,** 78, 1396.